Current Opinion in Solid State & Materials Science xxx (xxxx) xxx–xxx

Contents lists available at ScienceDirect

Current Opinion in Solid State & Materials Science

journal homepage: www.elsevier.com/locate/cossms

Recent advances towards applications of molecular bottlebrushes and their conjugates

Sidong Tu, Chandan Kumar Choudhury, Igor Luzinov*, Olga Kuksenok*

Department of Materials Science and Engineering, Clemson University, Clemson, SC 29634, United States

ARTICLE INFO

Keywords:
Molecular bottlebrushes
Grafting density
Degree of polymerization
Phase separation
Thermal stabilization
Strain-adaptive stiffening
Strain-induced coloration

ABSTRACT

We focus on the most recent developments towards synthesis, modeling, and applications of molecular bottlebrushes. Unique structural characteristics and properties of the bottlebrushes along with an ability to synthetically tailor their structure and functionality open up a number of emergent applications of these polymer systems. The conformation and resulting properties of molecular bottlebrushes and multi-component assemblies encompassing bottlebrushes can be regulated via chemical nature of the backbone and side moieties of bottlebrushes, variation of the distance between grafting points of the side groups, and the degree of polymerization of the side chains. Herein, we highlight the most recent progress in relating the structure of the bottlebrushes with their properties and focus on a number of diverse emerging applications involving bottlebrushes in solvents, melts, and bottlebrushes conjugated with surfaces, interfaces, linear chains, or biomacromolecules. Among such applications are drug delivery and sensing applications, electronic and photonic materials and materials with strain-adaptive stiffening, thermal stabilization and enhancement of activity of enzymes conjugated with copolymer bottlebrushes, and surface modification for biomedical applications.

1. Introduction

Molecular bottlebrushes, a special case of graft copolymers, also referred to as cylindrical polymer brushes, or molecular brushes, are linear macromolecules with relatively long side chains anchored to the backbone at high grafting densities [1–4]. Molecular bottlebrushes typically have relatively high chain stiffness due to excluded volume effects [1–4]. Several decades ago an analogy had been made between this structure and that of a 'bottle brush', where the grafted chains represent the bristles and the backbone represents the central wire support [5,6]. The unique shape and an ability to control the dimensions in a relatively straightforward manner are responsible for distinct properties of molecular bottlebrushes (MBBs). The conformation and behavior of MBB structure in bulk and solutions can be carefully regulated via chemical nature of backbone and side moieties, variation of the distance between grafting points of the side groups and the degree of polymerization of the side chains [7–14]. Molecular parameters for the brush-like polymers as well as the key definitions and phase diagrams are outlined in the recent studies [14]. The major structural parameters of the brush-like materials are the degree of polymerization of the bulky side chains, and the degree of polymerization of the backbone spacer between the side chains. When a certain application is aimed, these parameters are the major design elements targeted during the MBB synthesis along with chemical composition of the macromolecules and their molecular weight. The major strategies for the synthesis of bottlebrushes of different architecture (Fig. 1) are now well developed [4,7–11].

The bottlebrushes were first recognized as a distinct class of polymer materials in 1980s [7,10]. However, only in 21st century, when effective synthetic strategies for MBBs have been identified as well as advanced characterization tools (high resolution scanning probe, transmission and scanning electron microscopies) became readily available, unique application niches for MBBs have been being proposed and realized [7–12]. Despite an enormous progress in theoretical and computational studies of MBBs [13–21], derivation of an accurate correlation between the architectural characteristics of the bottlebrushes and their physical properties still remains a significant challenge. A large number of model parameters and interactions on various length scales constitute major roadblocks in developing accurate structure-property relationships. Herein, we will focus on a few recent advances in this direction, from a diagram of states in melts identifying different regimes corresponding to combs and bottlebrushes [21] to a recent study on thermodynamic, conformational, and structural properties of bottlebrushes as compared with different architectures, such as star and ring polymer melts [22].

To date, a number of comprehensive reviews has been devoted to

* Corresponding authors.
E-mail addresses: luzinov@clemson.edu (I. Luzinov), okuksen@clemson.edu (O. Kuksenok).

https://doi.org/10.1016/j.cossms.2019.01.003
Received 5 November 2018; Received in revised form 17 January 2019; Accepted 19 January 2019
1359-0286/ © 2019 Elsevier Ltd. All rights reserved.

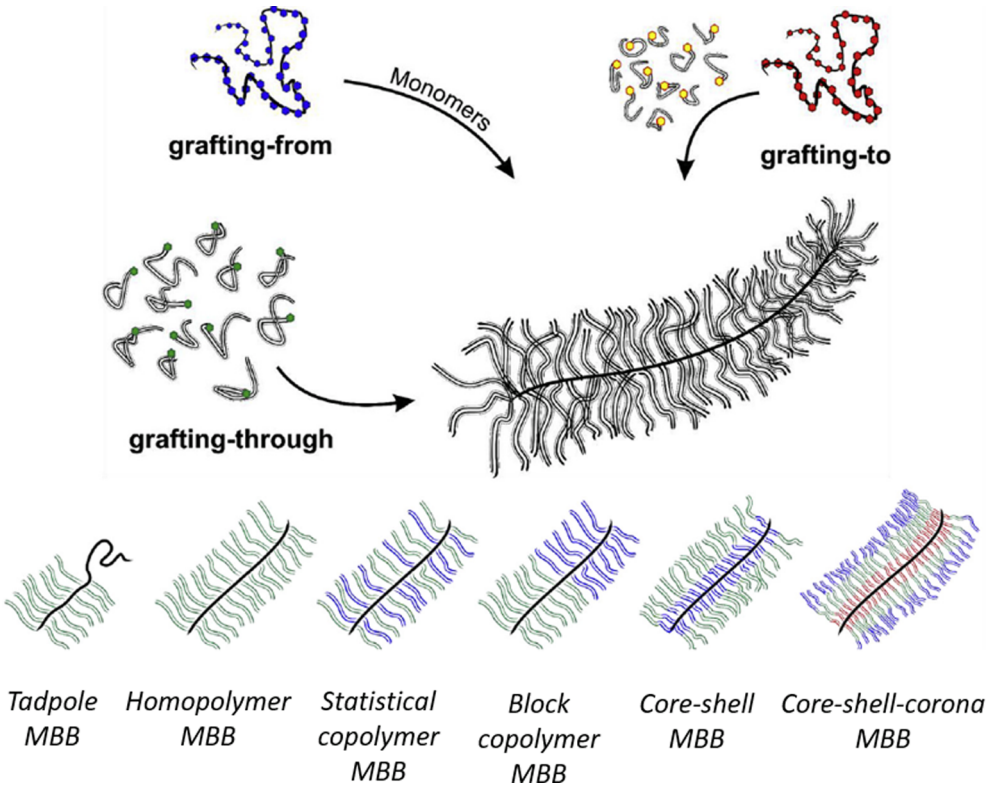

Fig. 1. Schematic representing three synthetic strategies used to obtain MBB (top row) and possible MBB macromolecular architectures (bottom row). Reprinted from Ref. [7]. Copyright (2016), with permission from Elsevier.

synthesis, structure, physical properties and applications of bottlebrushes [4,7–11,23–28]. These reviews offer a broad overview in historical prospective of the state of affairs in this specific area of polymer science. To this end, this mini-review focuses primarily on most recent theoretical and experimental results. We will first overview current theoretical and computational modeling of molecular brushes. Then we will present synthetic procedures that are presently employed for the MBB synthesis. Finally, we will focus on emerging applications of bottlebrush macromolecules and their conjugates.

2. Theoretical and computational modeling of molecular brushes

A combination of theoretical modeling often with the focus on scaling analysis and computer simulations aim to relate the molecular structure of the bottlebrushes and the chemical nature of their monomers with the physical properties of their solutions, melts, or cross-linked networks. Despite an enormous progress in understanding the structure and dynamics of bottlebrushes [13–22], this is a challenging problem and a number of open questions remain to be answered. The characteristic molecular dimensions of molecular bottlebrushes (and ultimately the properties of their solutions and melts) are controlled by the following three structural (or architectural) parameters: degree of polymerization of the side chains, N_{sc}, grafting density of the side chains, z, defined as a number of the side chains per backbone monomer, $z = 1/N_g$, where N_g is a degree of polymerization between the grafting points, and a degree of polymerization of the backbone, N_{bb} (see Fig. 2). For the case of the cross-linked network of molecular brushes, instead of N_{bb}, the third structural parameter controlling the properties of the bottlebrushes is the degree of polymerization of polymer strands between the crosslinks, N_x [20]. In addition to these structural parameters, the conformations and resulting properties of the bottlebrushes also depend on the chemical nature of the monomers (bond length l, monomer excluded volume v, and Kuhn length b) and on the affinities between the monomers constituting bottlebrushes and solvent molecules. The major challenges in capturing the behavior of the bottlebrushes and calculating their characteristic dimensions and rigidities steam from the interplay between contributions from various interactions over multiple length scales.

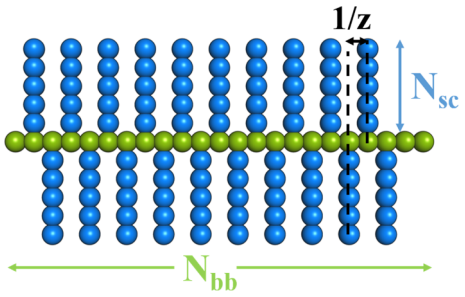

Fig. 2. Schematic of a bottlebrush architecture: N_{bb} and N_{sc} are degrees of polymerization of a backbone and a sidechain, respectively, and z is a grafting density.

2.1 Bottlebrushes in solutions

Bottlebrushes in solutions are characterized by the persistence length l_p, which represents the tendency of the chain to point in a particular direction and defines its rigidity, and by the radius of their cross section, R_{sc}. Notably, defining an effective persistence length in bottlebrushes is not necessarily straightforward [6]. A high-coverage limit corresponding to the bottlebrush regime defined by Fredrickson in early nineties required that the number of the side chain molecules per backbone monomer exceeded $N_{sc}^{-3/5}$ significantly [16]. In this case, the bottlebrush was expected to behave like a rigid rod if its dimensions were comparable to the persistence length, $l_p \propto N_{sc}^{15/8}$, while the long chains with $lN_{bb} \gg l_p$ were expected to undergo a self-avoiding random walk with the chain size scaling as $\propto z^{17/20} N_{sc}^{3/4} N_{bb}^{3/5}$. In the low-coverage

ARTICLE IN PRESS

limit, the chains were expected to assume comb-like configurations. Despite of the significant progress in understanding behavior of bottlebrushes in dilute solutions, an exponent a in the scaling of the persistence length $l_p \propto N_{sc}^{a}$ is still debated in the literature [14], taking values (in a good solvent) ranging from [29] 3/4 to the 15/8 discussed above [16]. Recent Molecular Dynamic (MD) simulations by Chatterjee and Vilgris [19] indicated a cross-over from the slower growth with $a = 3/5$ at low values of N_{sc} to the faster growth at $a = 15/8$ at high N_{sc} (or in the high coverage regime, with the bottlebrushes exhibiting semi-flexible toroidal structures).

In dilute solutions, the mean-square end-to-end distance, $\langle R^2 \rangle$, scales with the backbone degree of polymerization, N_{bb}, as , with the scaling exponent $\nu \approx 0.588$ supported by a number of simulations studies [16,22,30–32]. Notably, the best-fit value of ν is shown to be higher than the above value in simulations focusing on relatively short chains. For example, in Monte Carlo simulations by Elli et al. [33] the best fit values of ν were found to be 0.67 and 0.7 for grafting densities $z = 0.5$ and 1, respectively, for N_{bb} ranging from 10 to 100 with $N_{sc} = 5$. Theodorakis et al. [30] showed that relatively long chains need to be chosen to satisfy the $\nu = 0.588$ in the above scaling. In the latter MC simulations, long chains with the degrees of polymerization up to $N_{bb} = 1027$ were used and an effective persistence length was defined [30]. Note that a universal scaling is expected when a degree of polymerization approaches infinity, hence the deviations from the above exponent at low degrees of polymerizations is not surprising. The exponent ς describing the dependence of the root mean-square end-to-end distance, $\langle R^2 \rangle^{1/2}$, on the sidechain degree of polymerization, N_{sc}, as $\langle R^2 \rangle^{1/2} \propto N_{sc}^{\varsigma}$, was shown to depend on the bottlebrush architecture. For example, ς significantly increases with an increase in N_{bb} until it reaches saturation values of $\varsigma \approx 0.65$ and $\varsigma \approx 0.75$ at grafting densities of $z = 0.5$ and $z = 1$, respectively, at $N_{bb} \approx 300$, for the bond fluctuation model; even larger exponents up to $\varsigma \approx 0.88$ are found for the bead-spring model [30]. As another example, Paturej and Kreer estimated the dependence of the root mean-square end-to-end distance in the dilute solutions as [32] $\langle R^2 \rangle^{1/2} \propto (1 + N_{sc} z)^{2/5} N_{bb}^{3/5}$, assuming a semi-flexible backbone within an effective cylinder of a radius R_{sc} (valid for not extremely high $N_{sc} z$) and demonstrated a reasonable fit of this expression for a range of MD simulation parameters.

To date, the concentration dependence of the structure of the bottlebrushes received considerably less attention. Early work by Birshtein et al. [29] and Borosov et al. [15] identified three different scaling regimes for the size of the bottlebrushes as a function of their concentration, c. Recently, Paturej and Kreer [32] identified four different regimes characterizing scaling of the equilibrium mean-square end-to-end distance as a function of concentration of bottlebrushes in solution, c, as $\langle R^2 \rangle \propto c^{a}$, where the exponent a was shown to take values from $-1/4$ to $-4/5$. The authors attributed the difference between the four regimes to the hierarchical screening of the excluded volume interactions on different length scales. At lowest concentrations slightly exceeding an overlap concentration, an excluded volume screening was observed at the length scale of a backbone, resulting in $a = -1/4$ (same as in Ref. [34]), then further increases in c resulted in the screening on the smaller length scales [32] and corresponding increases in the value of an exponent a.

A particular interest with respect to designing responsive systems represents modeling of responsive molecular brushes. Recent coarse-grained molecular dynamics (CG MD) studies by Pannuzzo et al. [35] focused on the bottlebrushes with relatively hydrophobic backbones with a variable hydrophilicity of the side chains from hydrophilic to relatively hydrophobic. The authors quantified coil-to-globule transition observed with reduction in solvent solubility through the evolution of the radius of gyration for different architectures (including alternating chains of different length) but keeping the grafting density constant.

2.2 Bottlebrushes in melts

Daniel et al. identified four different regimes for comb and bottlebrushes in melts [14] depending on the grafting density, $z = 1/N_g$. At low grafting densities, loosely grafted combs with sparsely distributed side chains ($N_g > N_{sc}$) and densely grafted combs ($N_g < N_{sc}$) regimes were isolated. An increase in grafting density above the critical value results in the crossover to loosely grafted and then to densely grafted bottlebrushes. Importantly, in combs both backbone chains and side chains remain in unperturbed Gaussian conformations, while in bottlebrushes, high grafting density results in the strong steric repulsion causing an extension and an increased rigidity of the backbone. As a result, the bottlebrushes in melts adapt wormlike conformations and can be represented by the non-overlapping flexible filaments [14]. Theoretical arguments for the scaling of the persistence length with the radius of the filament as $l_p \sim < R_{sc}^2 >^{1/2}$ and with the backbone root mean- square end-to-end distance scaling as $\langle R^2 \rangle^{1/2} \propto N_{bb}^{1/2} N_{sc}^{1/4}$ are supported by the CG MD simulations [13].

Further, Liang et al. [21] defined a crowding parameter, Φ, as a volume fraction of monomers in the pervaded volume of side chains along the polymer backbone. This definition results in a clear distinction between the combs, where polymer chains overlap with $\Phi < 1$, and bottlebrushes at $\Phi \geq 1$, when the bottlebrushes no longer overlap and can be considered as semi-flexible filaments. Fig. 3 shows the diagram of state in the parameter space (φ^{-1}, N_{sc}), where the composition parameter $\varphi^{-1} = 1 + N_{sc}/N_g$ describes an effective "dilution" of the backbone. This diagram of states identifies three different subregimes of a bottlebrush regime: stretched backbone subregime (SBB), with the backbone stretched within the effective cylinder; stretched side chain subregime (SSC), where both the side chains and the backbone are stretched, and rod-like side chain subregime (RSC), where the side chains are fully stretched [21,36]. The chemical structure of a graft polymer restricts the maximum number of the side chains grafted to a backbone, and is responsible for the "Forbidden Region" in Fig. 3, so that the parameter space for SSC and RSC subregimes is relatively narrow [36]. Concurrent CG MD simulations supported the theoretical state diagram in Fig. 3 and showed [21] that the backbone mean-square end-to-end distance is a universal function of the above crowding parameter Φ. An important outcome of this study is that the crowding parameter Φ combines both architectural parameters of the brush and parameters characterizing the chemical nature of the monomers.

The rheological properties of MBBs are controlled by their architectural parameters. It was shown that the linear viscoelastic responses

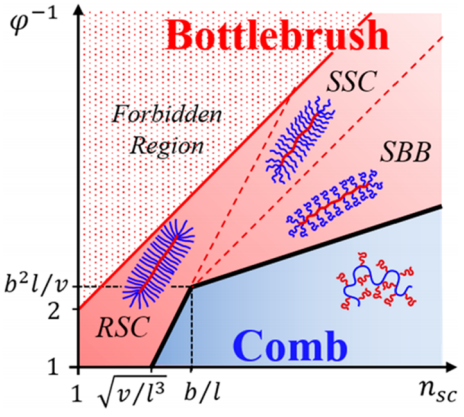

Fig. 3. Diagram of states of graft polymers in melts (logarithmic scales). SBB (stretched backbone), SSC (stretched side chain), and RSC (rod-like side chain) represent different subregimes of the "Bottlebrush" regime (in red), respectively; the "Comb" regime is marked in blue . The "Forbidden Region" marks the region inaccessible due to a chemistry of the backbone, which restricts a maximum number of side chains per monomer. Reprinted with permission from Ref. [36]. Copyright (2018) American Chemical Society.

of bottlebrush polymer melts encompass contributions from the characteristic relaxation modes of sidechains and entire brush molecules [37,38]; hence, these modes can be tuned by tuning the architectural features of the MBBs. It is known that entanglements of polymer chains result in a plateau of an elastic storage modulus. The ratio between the plateau modulus of a graft polymer melt and that of a linear chains melt was recently shown to be a universal function of the above crowding parameter Φ [36]. Further, the normalized plateau modulus as a function of grafting density was also measured for the bottlebrushes with dissimilar backbone and side chains [39]. The authors observed a transition from the comb to the dense bottlebrush without an indication of the loose bottlebrush regime; they however noted that the relatively low degree of polymerization could compromise quantitative comparison with the theory [39]. We also note that the theory was developed for the chemically identical monomers comprising the backbone and side chains; hence this theory should be modified when this assumption no longer holds. The homopolymer and copolymer experimental data can be collapsed into the universal master curve provided that the crowding parameter is normalized by its crossover value [36]. There is notable deviation of experimental data points from this universal curve within the crossover region between the comb and bottlebrush regimes; a variation in monomer density around grafting points could be one of these reasons for this deviation [36].

In the recent study by Jacobs et al. [40], the surface tension of the MBBs polymers was mapped using the same state diagram (Fig. 3). It was shown that the entropic corrections to the surface tension due to the redistribution of the grafting points and ends at the interfaces play an essential role at the bottlebrushes/vacuum interfaces; in contrast, the interfacial tension between linear melts and bottlebrushes is dominated by the enthalpic contributions [40].

Notably, bottlebrushes in polymer melts exhibit a number of similarities in their structural characteristics and some of the properties with ring polymers and stars with the moderate number of arms (five to six) [22]. These similarities extend to segmental density, isothermal compressibility, isobaric expansion, and to similar scaling tendencies of the radius of gyration and hydrodynamic radius. Finally, the eigenvalues of the radius of gyration calculated in the same work allowed the authors to quantify the shapes of the bottlebrushes in melts depending on the degree of polymerization of the side chain and to clearly identify ellipsoidal or star-like ($N_{bb} < N_{sc}$), spherical ($N_{bb} \sim N_{sc}$), and anisotropic ($N_{bb} \gg N_{sc}$) shapes. We note that along with the grafting density typically used to characterize bottlebrushes, the authors also defined segmental density that effectively allows one to compare packing efficiency of different chain architectures (bottlebrushes, rings, and stars).

2.3. Computational modeling of bottlebrushes

We have already discussed a number of examples of simulations of bottlebrushes in the above sections; in these examples, simulations largely served to validate theoretical arguments such as various scaling arguments. We now briefly summarize computational approaches that are often used to model molecular bottlebrushes and highlight some of available comparison between recent simulation studies and experimental results. The simulation approaches used to study MBBs mainly encompass self-consistent field theory (SCFT) [17,41], Monte Carlo (MC) [31,33,42], coarse-grained molecular dynamics (CG MD) simulations [13,14,19,30,32], and, more recently, dissipative particle dynamics (DPD) simulations [43–45]. Hsu et al. performed Monte Carlo simulations of bottlebrushes focusing on their structural features and compared simulation results with the available experimental data [6,31,46]. These authors used MC simulations along with theoretical arguments to assess the applicability of the Kratky-Porod wormlike model for the polymers in solvent in two and three dimensions and showed that while this model is applicable for relatively stiff and thin polymers, it does not describe relatively thick bottlebrushes. They have pointed out that despite drawbacks of the Monte-Carlo simulations on a lattice resulting in the self-avoiding walks with an additional energy penalty for bond-bending, the simulation results for the normalized mean-square radius of gyration $\langle R_g^2 \rangle / 2 l_p L$ as a function of the number of Kuhn segments n_K showed a striking similarity [46] with experimental data by Norisuye and Fujita [47]. Leuty et al. [48] used the bead-spring model in CG MD to show the effects of the side chain length and grafting density on the nature of tension amplification in layers of bottlebrush tethered to a surface. These simulation results supported earlier theoretical predictions [2,49] that tethering MBBs to a solid substrate leads to a significant amplification of tension in the linker above a surface coverage $\Sigma^{**} \approx 1/R_{sc}^2$ associated with the side chain size. Zhang et al. [50] focused on the structure and dynamics of a bottlebrush-like polymer using atomistic MD simulations and showed its transition from a flexible chain to a compact form. While the authors indicated a few shortcomings of their approach, from the limited time scales common to all MD approaches prohibiting capturing dynamic features on larger time scales, to somewhat artificial initial structures in their simulations that may not reflect the stretched side chains realistically, they nonetheless showed a very good agreement between scattering intensities calculated at longer simulation times and that from experimental SANS [50]. Chremos and Theodorakis [51] probed the self-assembly of bottlebrush block copolymers by CG MD simulations of a bead-spring model and analyzed the morphologies of copolymers with various molecular architectures. Gu et al. [52] used dynamic Metropolis MC and a strong segregation theory to study the self-assembly of bottlebrush block copolymers and showed a good agreement between the scaling of the interlamellar spacing with backbone degree of polymerization obtained in simulations and in the concurrent experimental studies.

Another approach that is widely used to simulate dynamics of various polymeric systems is dissipative particle dynamics (DPD) approach [53]. DPD is a coarse-grained approach that affords larger time steps making larger systems computationally accessible compared to MD though the chemical specificity is lost. In effect, DPD can be thought of as an isotropic Galilean invariant thermostat that accurately reproduces hydrodynamic interactions [54]. Yan et al. employed a DPD approach to investigate the cylindrical polyelectrolyte brush in the presence of multivalent counter ions and showed that the excluded volume effects of these ions increase the cylindrical polyelectrolyte brush size [43,44]. Teng et al. used DPD to investigate the surface segregation of binary athermal bottlebrush/linear polymer blends in a nanoscale thin film [45]. Our DPD simulations of the bottlebrushes shown in Fig. 4 agree with the well accepted scaling for bottlebrush mean-square end-to-end distance in a good solvent, $\langle R^2 \rangle^{1/2} \propto N_{bb}^{0.6}$. We note that the first point on this plot with the shortest chain ($N_{bb} = 20$) is excluded from the

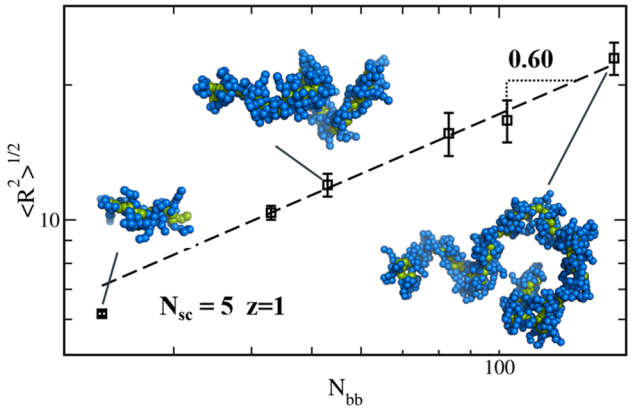

Fig. 4. Root mean-square end-to-end distance of bottlebrushes in solvent (DPD simulations). An initial configuration is given in Fig. 2 with z = 1 and $N_{sc} = 5$. The insets show late time snapshots of MBBs configurations for the chosen values of N_{bb} as marked by the arrows. Each data point is averaged over four independent simulation runs.

fitting. In these simulations, we set an initial configuration as shown in Fig. 2, with N_{sc} = 5 and grafting density z = 1, and varied N_{bb} from 20 to 150; the DPD simulation parameters for the polymer beads and solvent are the same as in Ref. [55].

3. Synthesis of molecular bottlebrushes

There is a significant amount of practical information available on synthesis of molecular bottlebrushes, which is summarized in a number of comprehensive reviews [4,7–11,23–28,56]. In a course of synthesis the major target is to control and regulate degree of polymerization of the backbone spacer between the bulky side chains, chemical composition of the backbone and side chains as well as their degree of polymerization. In the past few years, the key advancements in the synthesis of bottlebrushes focused mostly on optimizing the methods already available to obtain well-defined MBBs rather than in the direction of development of novel synthetic strategies/methods. In terms of strategy the grafting-through [12,56–72], grafting-from [67,73–86] and grafting-to [68,82,87–90] synthetic procedures continue to be widely used to tailor MBBs for certain applications (Fig. 1). The advantages and disadvantages of each method are well understood [7,8,10]. In the grafting-through approach, macromonomers are first prepared to be polymerized to form the bottlebrushes. The grafting-from method is based on the polymerization initiated from the pre-synthesized MBB backbone to obtain the side chains. Finally, according to the grafting-to synthetic strategy, the side chains and backbone are synthesized separately and then the side chains are anchored to the backbone via high-yield coupling reactions. Using the above- mentioned approaches and their combinations, MBBs possessing various chain architectures (from homopolymers to core-shell copolymer) have been synthesized (Fig. 1) [7,8,10,26,27,56,59,75].

As of today an extensive portfolio of chemical coupling reactions and polymerization procedures is developed and effectively employed to obtain MBBs of different architectures and chemical compositions [4,7–11,23–27]. Currently, the conventional and controlled radical polymerization of macromonomers containing reactive unsaturated bonds [12,58,62,63,65,67,71,73] and ring opening metathesis polymerization (ROMP) of norbornenyl macromonomers [56,57,59–61,64,69,70,72] are the most employed in the grafting-through method polymerization techniques. In addition, polymerization of di-trimethylsilylacetylene-benzene macromonomers [66] and benzofulvene derivatives [68] were carried out to obtain brush–like polymers using grafting-through approach. Controlled radical [67,73–81,83,86] and ring opening polymerizations (ROP) [84–86] are the most used in the grafting-from approach techniques. Anionic living polymerization was also used for grafting of side chains to syntesyze MBBs [91]. Various high yield coupling reactions are utilized to anchor the side chains to backbone in the grafting-to synthetic methodology. Among there reactions are thiol-epoxy coupling [88], reaction of living anionic chains with functional groups located on the backbone [82,90], and azide-alkyne cycloaddition (click reaction) [68,87,89].

4. Emerging applications

The unique MBB chain architecture leads to a number of their unusual and potentially valuable morphological characteristics and properties [7,8,10,26]. The polymers can attain cylindrical or worm-like conformations and extraordinary spatial configurations. Consequently, a single bottlebrush macromolecule can adopt a size of a colloid. In contrast to linear polymers, MBBs having high molecular weight do not form extended and stable entanglements in bulk and solutions. This physical phenomenon is an origin of their quite distinctive mechanical and rheological properties. In addition, bottlebrush copolymers can self-assemble in structures with controlled domain sizes significantly more rapidly than linear block copolymers. Bottlebrush block copolymers can form micelles in a selective solvent at a significantly lower critical micelle concentration then their linear block copolymer analogs. The side-chains of MBBs can be readily tailored for interaction with a liquid media, solubility, or to carry some specific functional groups. In this respect, the highly branched MBBs are effective in modification/functionalization of surfaces and interfaces, since single MBB macromolecule located at a phase boundary allows for interfacial localization of a significant number of functional moieties. Moreover, the block-type MBBs display behavior analogous to the one of conventional block copolymers and can be employed as compatibilizers of polymer blends and mixtures.

4.1. Self-assembled structures for drug delivery, medical imaging, sensing, and biodetection

It is well established that MBB copolymers having blocks of different polarity can form true solutions or micellar, bilayer, cylindrical, and nanoparticle structures with significant thermodynamic stability [7,8,10,26,73]. The structures are typically larger than the ones formed by linear diblock copolymers and can have an extra functionality incorporated in their side-chains without compromising the stability of their structures. The applications of the self-assembled structures are envisioned in stabilization of emulsions, drug delivery, medical imaging, sensing, and biodetection.

To this end, Motoyanagi et al. reported on synthesis and properties in liquid media of brush-shaped conjugated polymers consisting of a poly(phenylene butadiynylene) backbone and poly(vinyl ether) (polyVE) side chains, poly(DE-PIBVE_n) (Fig. 5a) [66]. The solution of the macromolecules with a specific side chain length exhibited

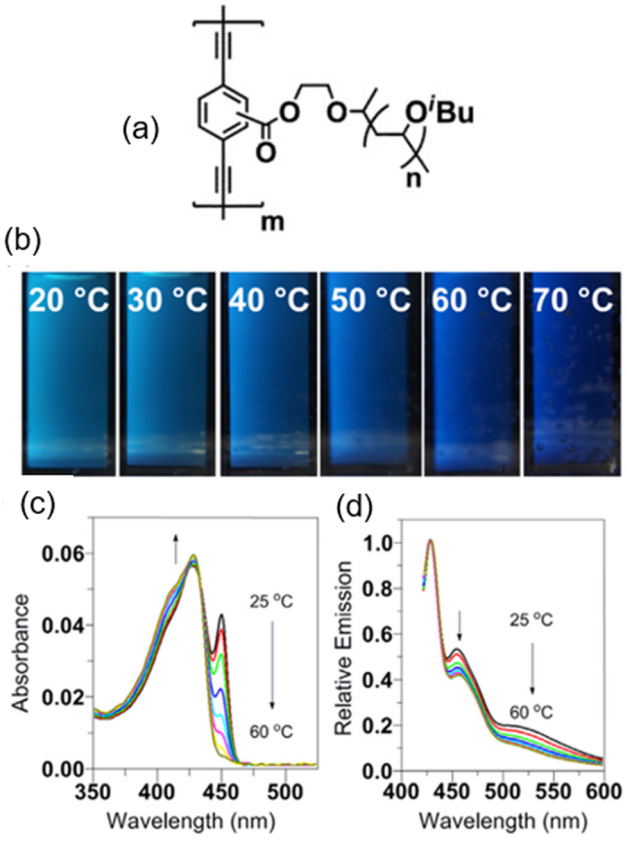

Fig. 5. Thermochromism of molecular brushes: (a) chemical structure of polyDE-PIBVE_n; (b) fluorescence images, (c) UV-vis spectra and (d) fluorescence spectra of polyDE-PIBVE_{15}) in AcOEt under the temperature control from 25 to 60 °C (λ_{ex} = 420). Republished with permission from John Wiley and Sons, from Ref. [66]; permission conveyed through Copyright Clearance Center, Inc.

solvatochromism and thermochromism depending on the chemical nature of the media employed and can be used in sensor applications. To this end, Fig. 5b shows that the fluorescence color of poly(DEPIBVE$_{15}$) continuously changed from skyblue to dark-blue with the increase in temperature. The visual observations are corroborated by temperature dependencies of the UV–vis absorptions and fluorescence spectra of the polymer solution taken at different temperatures, Fig. 5c and d. It was pointed that thermochromism could be induced by the dissociation of the polymer aggregates into molecularly dispersed polymers with temperature increase. Thermoresponsive LCST (lower critical solution temperature) type behavior was also reported for poly [o-aminobenzyl alcohol-graft-poly(N-isopropylacrylamide)], [P(oABA-g-PNIPAM)] MBB [78]. The bottlebrush demonstrated higher LCST than that of its linear PNIPAM counterpart. PNIPAM-based cyclic molecular brush copolymer: poly(2-hydroxyethyl methacrylate-g-poly(N-isopropylacrylamide-st-N-hydroxyethylacrylamide)) [cb-P(HEMA-g-P(NIPAAm-st-HEAAm))] having a cyclic core of PHEMA and thermosensitive brushes of statistical copolymer of P(NIPAAm-st-HEAAm) has been considered for anticancer drug delivery [74]. LCST of the polymer was different than the one demonstrated by non-cyclic MBB analogue. The temperature transition was adjusted to be above the physiological temperature, but lower than the localized temperature of tumor tissue, to allow for pointed anticancer drug delivery. The drug-loaded cyclic MBB showed enhanced in vitro cytotoxicity than the non-cyclic MBB analogue.

Bottlebrush copolymer cross-linked micelles made from polylactide-*b*-poly(ethylene oxide) were tested as a vehicle for delivery of hydrophobic anticancer drug paclitaxel [57]. The micelles prepared from bottlebrush copolymers with branched PEO side chains demonstrated the highest paclitaxel uptake that was increasing with the size of PEO side chains. Mullner et al. studied how MBB shape-anisotropic PEGylated brush nanoparticles of different sizes/topology could associate with multicellular tumor spheroids (MCS) [79]. In essence, it was found that the nanoparticles with the aspect ratio of ~4–5 demonstrated higher association to MCS and improved penetration into the center of the spheroid. Another work related to MBB aided drug delivery study was devoted to tri-component polymer obtained by functionalizing the polybenzofulvene backbone with nona(ethylene glycol) (NEG) arms terminated with low molecular weight hyaluronic acid (HA) macromolecules [68]. The molecular brush formed stable nanoparticles in water that were devoid of cytotoxicity and could be studied further to serve as nanocarrier for drug delivery or material for tissue engineering.

4.2. MBB networks with strain-adaptive stiffening

Recently, Vatankhah-Varnosfaderani et al. [65] utilized the self-assembly of the linear-bottlebrush-linear triblock copolymers to develop a unique class of elastomers (also referred to as plastomers) that can exhibit extreme strain-adaptive stiffening along with strain-induced coloration. Remarkably, the mechanical properties of these plastomers can be tailored to closely replicate those of various biological tissues. This can be seen from Fig. 6a, in which the stress-elongation curves for various tissues (symbols) overlap with the corresponding stress-elongation curves for selected plastomers with various architectural designs. These plastomers are super-soft with apparent Young's modulus on the order of $E_0 \sim 10^3$–10^5 Pa and exhibit strain stiffening, $E_0^{-1}\partial\sigma/\partial\lambda$, on the order of 1–100 with the characteristic sigmoidal shape dependence on λ, similar to that observed in biological tissues.

During the phase-separation, aggregation of linear blocks forms physical crosslinks, with bottlebrush strands ensuring low elastic modulus; further, selecting the system that is in the strong segregation regime ensures pre-straining of the bottlebrush strands [65]. Under an applied stress, the two-stage deformation process is observed: during the first stage (purely elastic deformations), the pre-strained bottlebrush strands are stretched, and during the second stage, the linear chains forming relatively rigid domains within the soft matrix are uncoiled. Elongation also results in the blue shift of the sample's color (Fig. 6b) via an increase of the distance between the domains of coiled linear chains.

Ina et al. [92] varied the side chain grafting density and the cross-linking density of the brush-like solvent-free elastomers to control their elastic modulus within the range from ~1 to 100 kPa. The authors verified the crossover between the classical wetting and adhesion regimes by measuring spontaneous indentation depth of micrometer-sized particles and showed a good agreement between experimental results and results obtained from the computer simulations [92].

4.3. Enzymes-MBBs conjugates: Enhancement in stability and activity

Improving thermal stability of enzymes can bring a number of advantages of using enzymatic reactions at high temperatures [93,94]. Recent studies showed that conjugating molecular bottlebrushes with enzymes can significantly improve the thermal stability and activity of these enzymes [71,95,96]. Specifically, lysozymes conjugated with poly (glycidyl methacrylate-stat-oligo(ethylene glycol) methyl ether methacrylate), poly(GMA-stat-OEGMA) MBB copolymers (Fig. 7), had shown an increase in their thermal stability and catalytic activity above 100 °C. The copolymer chains were conjugated via the GMA moieties to the lysine residues of the lysozyme. These long copolymer MBBs enveloped multiple enzyme forming cocoons (AFM images in Fig. 7a and b and the schematic of cocoon formation with enzymes indicated in green in Fig. 7b) [71,95]. A fraction of the long polymer bottlebrush with the same monomeric constituents as used in experiments was constructed in concurrent MD simulations (Fig. 7d) [71]. The simulation box contained the conjugated enzyme, additional free-floating polymer chains mimicking effects of longer polymer chains, and water molecules (see Fig. 7e). The simulations of the conjugated lysozyme at the elevated temperatures with relatively high water concentration resulted in phase separation and formation of water and polymer-rich domains; the instant in time the Lysozyme became exposed to the water domain was shown to onset the unfolding process.

On the contrary, no phase separation was observed below the critical water content [95]. The structural stability analysis (RMSD in Fig. 5f (black lines), the number of intra-protein hydrogen bonds and a number of contacts) showed that the lysozyme retained its structural integrity in response to a temperature increase [95]. These results showed that restricting water access in the close vicinity of the enzyme promotes the structural stability of the lysozyme at high temperatures. The conjugation with the GMA moieties serves to provide confinement for the enzyme and ensures high polymer concentration in the close vicinity of the enzyme. While these studies provide a basis for designing a range of enzyme-copolymer conjugates with improved stability and activity, a number of questions remain open, namely the mechanism of prevention the agglomeration between multiple enzymes as well as effects of particular architectures of molecular brushes on stability and activity of conjugated structures. These questions could potentially be answered with the development of large scale coarse-grained models and further studies capturing multiple enzymes and long molecular brushes on larger length scales.

4.4. Pressure-sensitive adhesives and shape-memory materials

Phase-separated MBBs were recently evaluated for applications as pressure-sensitive adhesives [58]. Specifically, acrylic based adhesives containing polyester side-chain of different lengths were synthesized to investigate the effect of branching on phase separation and polymer mechanical performance. Ring-opening co-polymerizations of L-lactide (L-LA) and ε-caprolactone (ε-CL) initiated with 2-hydroxyethyl methacrylate (HEMA) was used to obtain the polyesters vinyl macromonomers. Then copolymers of the macromonomers with 2-ethylhexyl acrylate and acrylic acid were synthesized using conventional free-radical polymerization. It was found that the formation of distinct

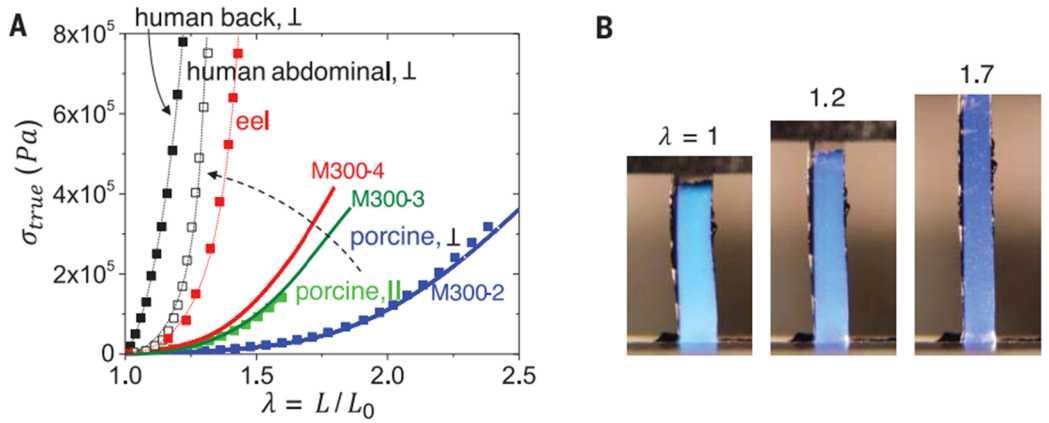

Fig. 6. (a) Stress-elongation curves for various tissues (symbols) and for selected plastomers (linear-bottlebrush-linear triblock copolymers) (solid lines). (b) Blue shift of the sample's color via an increase of the distance between the domains of coiled linear chains. From Ref. [65]. Reprinted with permission from AAAS.

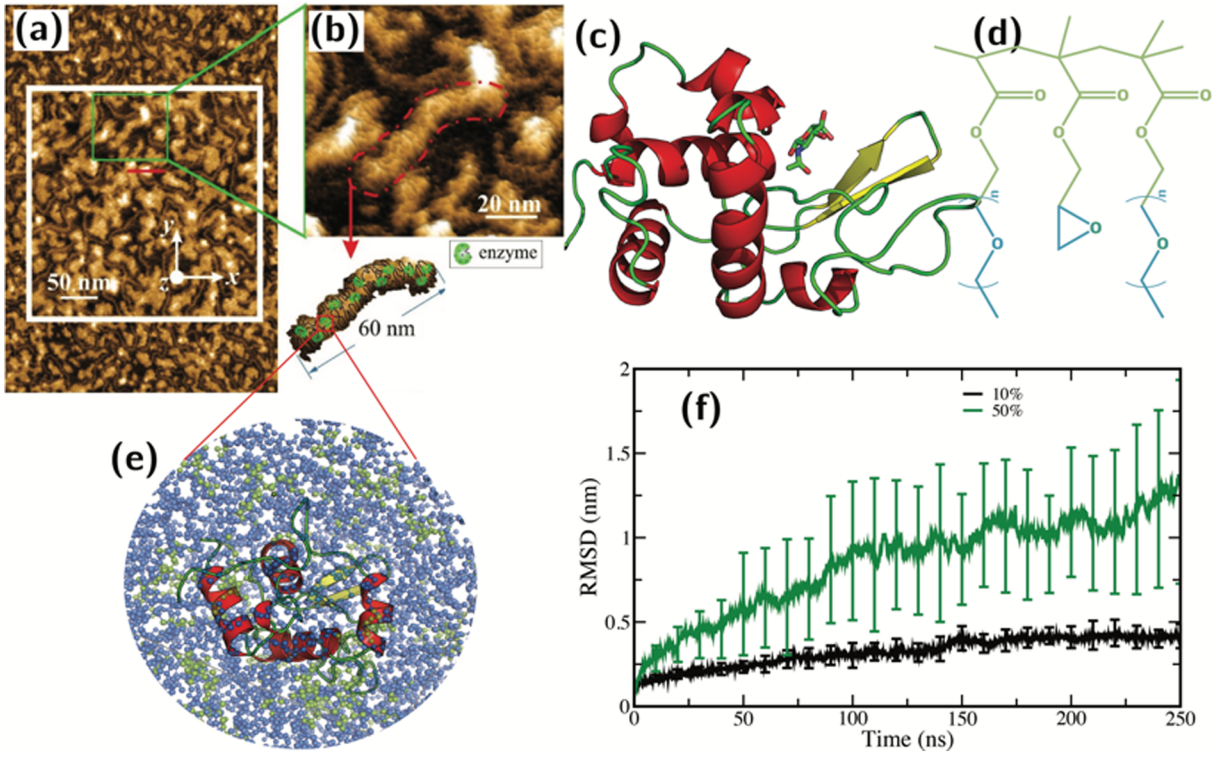

Fig. 7. (a and b) AFM micrograph of lysozyme-polymer conjugate. (c) Lysozyme (PDB ID = 1PJR) crystal structure, with alpha-helices, beta-sheets and turns in red, yellow and green, respectively. (d) The polymer structure used in simulations. Hydrophobic (glycidyl methacrylate, GMA) and hydrophilic (oligo(ethylene glycol) OEGMA) segments are shown in green and blue, respectively. (e) Equilibrated high temperature low-water content lysozyme-polymer conjugate. Lysozyme is surrounded by polymer chains. Water molecules are hidden. (f) Root mean-square displacement (RMSD) for high (50% w/w) and low (10%) water concentration systems at high temperature from the native crystal structure. (a) and (b) are reprinted with permission from Ref. [71]. Copyright (2017) American Chemical Society. (f) is reprinted with permission from Ref [95]. Copyright (2018) American Chemical Society.

microphases occurs with increasing side-chain lengths. Mechanical testing of the materials revealed that the increase of the side-chain molecular weight resulted in a noteworthy increase in both peel strength and shear resistance. Deshmukh et al. [60] reported on synthesis of shape-memory brush-like cross-linked polycaprolactones (PCLs) and their linear analogues. It was found that the difference in macromolecular architecture to a great extent influences physical properties of the PCL networks. Owing to the reduced entanglement the brush network exhibit four times lower rubbery modulus than the linear ones along with excellent shape memory performance.

4.5. MBBs for nanoporous materials

The ability of MBBs to self-assemble into submicron quasi-ordered structures have been utilized for generation of nanoporous organic polymer materials [83,84]. For instance, the core-shell bottlebrush copolymers were employed to fabricate well-defined organic nanotube network as catalyst support with high surface area and enhanced transport properties [84]. Specifically, the side chains of core-shell bottlebrushes were hyper-crosslinked with following selective removal of the MBB core (Fig. 8). The catalyst incorporated into the nanoporous material displayed outstanding catalytic performance and reusability. Yuan et al. utilized similar strategy where poly(*n*-butyl acrylate)-block-polyacrylonitrile MBB were pyrolyzed to form porous nitrogen-doped

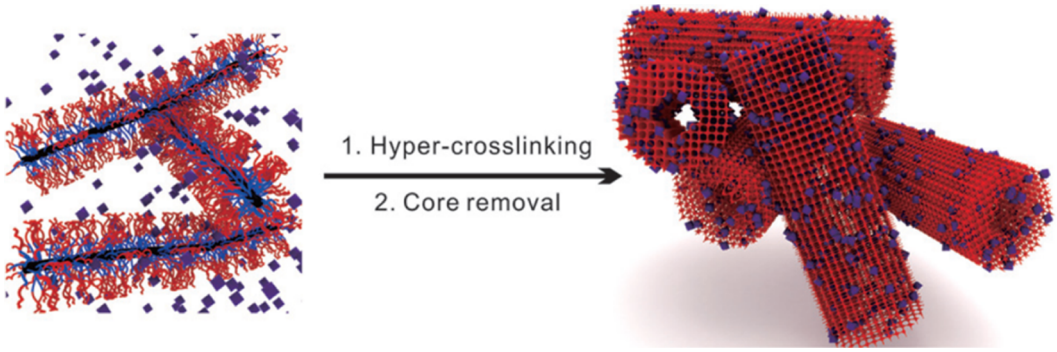

Fig. 8. Formation of catalyst supported on microporous organic nanotube networks. Reproduced from Ref. [84] with permission from the Royal Society of Chemistry.

carbon (420 m^2/g) for oxygen reduction reaction [83]. Prior to the pyrolysis polyacrylonitrile blocks were cross-linked and poly(*n*-butyl acrylate) blocks were decomposed. Brush-like triblock copolymers with norbornene backbone comprising functionalized amine monomers in the central block, side-chain liquid crystalline and side-chain polylactide end blocks were employed to fabricate functional nanoporous membrane [59]. The block copolymers self-assembly forming phase segregated nanostructured material. Via removal of PLA phase and crosslinking of the polynorbornene backbone amine-functionalized functional nanoporous membranes were obtained. According to the authors the membranes may find applications in filtration, catalysis, and sensing.

4.6. MBBs for electronic and photonic applications

There are at least three classes of MBBs being designed for electronic applications. The first class is constituted from the polymers possessing conducting/semiconducting backbones and/or side chains [27,69,70,87]. The second class is formed by the bottlebrush polymers having polyethylene oxide/polyethylene glycole (PEO/PEG) side chains [80,91]. Here the side chains are serving as “solid” polyelectrolytes carrying lithium ions. Finally, rubbery bottlebrushes are considered for application as dielectric elastomers [9,12]. Bottlebrushes were also employed as templates in fabrication of SnO_2-based electrodes for Li-ion batteries [81] and for formation of MBB/fullerene composite material for employment as an electrode interlayer in organic solar cells [97].

MBBs with conductive backbones and/or side chains are a promising class of materials to be used in organic electronics, sensors, stimuli-responsive surfaces, and biomedical applications [27,69,70,87]. Initial attention to such materials was driven by interest to improve solubility, mechanical properties and processability of conductive polymers. Nowadays it is also realized that synthesis of brush-like (semi)conducting polymers offers route to tailoring their conductivity, electrochromism and structural morphology, and consequently to designing efficient photovoltaic cells, electrochromic displays, light-emitting diodes (OLEDs), or organic field-effect transistors (OFETs) [27,70]. For instance, MBBs with rigid semiconducting poly(3-hexylthiophene), P3HT side chains and polynorbornene backbone were obtained and tested in heterojunction solar-cell devices [70]. It was determined that P3HT side chains having higher degree of polymerization possess better semiconducting properties resulting in higher solar-cell device performance. In another work devoted to P3HT, Heinrich and Thelakkat [87] obtained and tested series of well-defined bottlebrushes having polystyrene backbone grafted with P3HT chains. They found that crystallization was not observed for polymers with low molecular weight P3HT side-chains. These copolymers showed very poor electronic properties. The crystalline lamellar structures and the best charge transport properties were obtained with an increase of the side-chain length.

Zardalidis et al. [91] have reiterated that PEO is one of the best candidates to be employed as solid polymer electrolyte effective in dissolving metallic salts. However, the polymer does not have the necessary mechanical stability and modulus needed to prevent dendritic growth at the electrodes. To this end, they synthesized and studied poly (hydroxystyrene) (PHOS) densely grafted with PEO and its block copolymer with polystyrene (PS). It was found that the copolymers can produce Li ion conductivities that are similar to or even higher than in the respective PEO electrolytes. At the same time the copolymer based electrolytes demonstrated improved mechanical properties. Lyu et al. have also demonstrated that polyelectrolyte based on random binary brush copolymer composed of PEO and PS side chains provided both high ionic conductivity and high mechanical strength at room temperature [80].

Dielectric elastomers are an important class of polymers that are used to build polymer based systems responsive to an application of electric field [9,12]. Namely, upon exposure to electric stimulus the materials respond by changing size, shape or both. The major application of these materials have been to build artificial muscles due to a favorable combination of large stroke, fast response, and high energy density. For instance, Vatankhah-Varnoosfaderani et al. designed bottlebrush elastomers for the freestanding actuators that allow for large stroke ($>$ 300%) at low applied fields in unconstrained as-cast shapes [12]. The elastomers consisted of methacrylate backbone and poly(dimethylsiloxane) (PDMS) side chains and were synthesized by radical polymerization of macromonomers in the presence of cross-linkers. It was shown (Fig. 9) that the bottlebrush elastomer film undergoes more than 4 times areal expansion prior to electrical breakdown. The authors associate the superior behavior of MBB elastomer with elimination of polymer chain entanglement in the bottlebrush materials.

Rzayev had shown that bottlebrush copolymer melt separates into highly ordered lamellae domains; in these studies, high molecular weight polylactide/polystyrene bottlebrush copolymers were used and large domain spacings over 100 nm were achieved [86]. These studies pioneered applications of bottlebrush copolymers to fabricate photonic crystals. A recent review [56] highlights advances in tuning the properties of photonic crystals fabricated by the self-assembly of bottlebrush copolymers. Photonic crystals are ordered composites with periodicity comparable to the wavelength of light. A low entanglement, an ability to control domain spacing, and an exceptionally rapid self-assembly promoting the process of templating nanoparticles into the well-ordered domains makes these copolymers excellent candidates for photonic crystals with photonic bandgap tunable within the wide range [56,98].

4.7. MBBs for surface and interfacial modifications

Examples of MBBs applications for surface and interfacial modifications include their employment in antifouling/antimicrobial coatings [67,77,99], regulation of cell adhesion [62], inhibition of ice

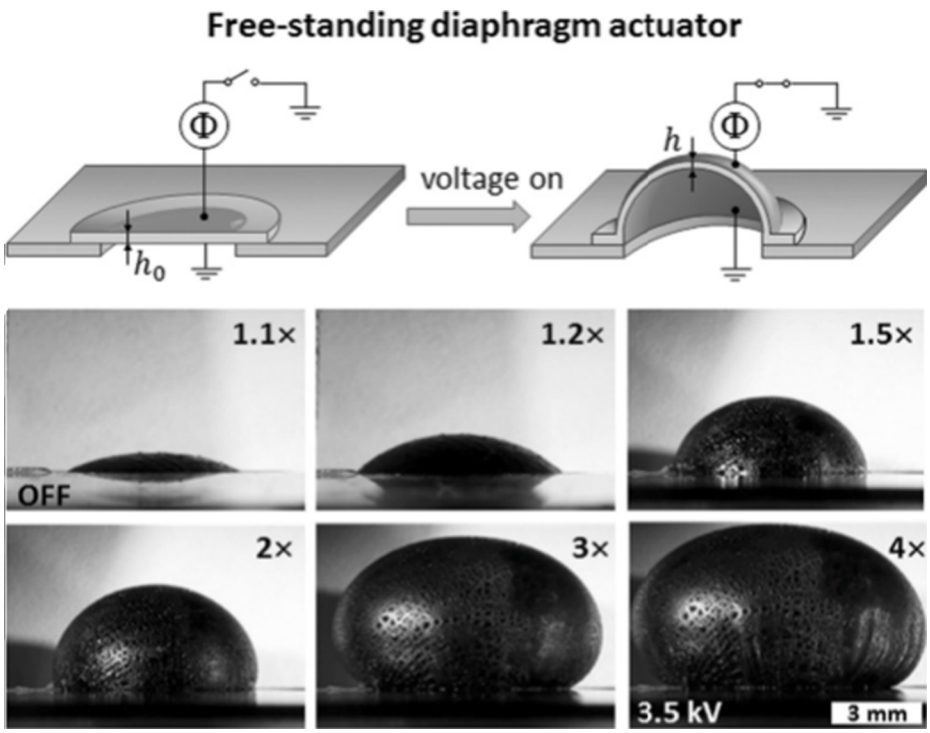

Fig. 9. *Top*: Schematic for operation of freestanding dielectric elastomer diaphragm actuator, where deflection of a circular diaphragm upon electroactuation with increasing voltage is observed. *Bottom:* deflection of circular diaphragm, made of elastomer having methacrylate backbone and poly (dimethylsiloxane) side chains, (h_0 = 0.44 mm) is evident upon electroactuation with increasing voltage Φ. The numbers indicate field-induced areal expansion $\lambda_a = A/A0 = h_0/h$ under isochoric conditions. Republished with permission of John Wiley and Sons, from Ref. [12]; permission conveyed through Copyright Clearance Center, Inc.

crystallization [76], surface lubrication [75], regulation of wettability [61,64], and modification of graphene oxide (GO) [62,63]. For instance, Faivre et al. studied tribological properties of a number of bottlebrushes having a central brush block composed of poly(2-methacryloyloxyethyl phosphoryl choline) side chains and an adhesive block made of quaternized poly(2-dimethyalminoethyl methacrylate)-*co*-poly(methyl methacrylate) [75]. Performance of MBBs with different chain architectures (monoblock possessing only the bottlebrush central block, a diblock copolymer having one lateral adhesive block, and a triblock copolymer with two lateral adhesive blocks) was contrasted. Using the surface force apparatus, it was found that the presence of the adhesive blocks does not impact the friction coefficient. However, the MBBs with two adhesive blocks demonstrated drastically increased threshold pressure at which wear was initiated. Pesek et al. showed that MBB with PDMS and PLA mixed side-chains can be used as an effective hydrophobic additive for PLA matrix [64]. The bottlebrush spontaneously segregate to the PLA boundary and is more efficient surface-active material than PLA-*b*-PDMS diblock copolymer and pure PDMS. The noteworthy hydrophobicity was also reported for fluorinated bottlebrushes possessing poly(2,2,2-trifluoroethyl methacrylate) side chains [61]. The authors associate the enhanced hydrophobicity of MBBs with enrichment of the surface with fluorine containing end groups due to the side chain crowding effect.

Molecular bottlebrushes containing PEG/PEO units in side chains have been shown to be valuable materials for biomedical/bioengineering surface related applications. To this end, MBB block copolymers comprised of antimicrobial (polyhexamethylene guanidine), antifouling (PEG), and surface-tethering segments in one molecule were synthesized and grafted to silicon rubber via plasma/autoclave-assisted method [99]. The materials demonstrated significant antimicrobial and antifouling activity in *in-vitro* and *in-vivo* tests. Xu et al. showed that the molecular brushes consisting of PEG, fouling-release hydrophobic poly (2,2,3,3,3-pentafluoropropyl acrylate), and catechol anchoring moieties deposited on inorganic surface are capable to significantly reduce unwanted protein adsorption and cell adhesion [67]. In another example, amphiphilic asymmetric MBBs containing side chains made of PS and PEG were used to fabricate effective antifouling surfaces as well [77].

Borodinov et al. synthesized molecular brush copolymers made of GMA, OEGMA and lauryl methacrylate (LMA) by conventional free-radical polymerization [62]. These copolymers can be used to obtain functional grafted brush-like layers via reaction of GMA units with a surface located functionalities. It was shown that accurate control over cell (osteoblasts) adhesion and growth can be achieved using the anchored surface layers made of PGMA, P(GMA-LMA), P(GMA-OEGMA), and P(GMA-OEGMA-LMA) macromolecules (Fig. 10). Specifically, the attachment and spreading of osteoblast was shown for PGMA and P (GMA-LMA) grafted layers. Conversely, practically no cell adhesion was observed for the P(GMA-OEGMA) MBB coating, owing to high percentage of PEG-containing components. The P(GMA-OEGMA-LMA) MBB grafted film represents important intermediate case, where osteoblast attachment took place while no proteins were adsorbed on the surface. It is important to emphasize that all four polymer systems demonstrated high biocompatibility and low cytotoxicity resulting in little to no evidence of non-viable osteoblasts attached to the samples. These molecular brush copolymers can be also employed to control the deposition of graphene oxide sheets on both hydrophilic [GO modified with P(GMA-OEGMA)] and hydrophobic [GO modified with P(GMA-OEGMA-LMA)] surfaces [62,63]. Specifically, it was found that the grafting of the molecular brushes to GO surface allows formation of GO monolayers on surfaces of various polarity via dip-coating from water (Fig. 11).

5. Conclusions and outlook

In this mini-review we have highlighted the most recent developments towards synthesis, modeling, and applications of molecular bottlebrushes. Recent theoretical and experimental studies of molecular bottlebrushes and conjugates incorporating MBBs are paving the ways for a number of emergent applications of these polymer systems. Unique properties of molecular bottlebrushes and an ability to synthetically tailor their functionality by varying the structural parameters result in MBB applications in materials with adaptive functionality or specific properties that can resemble some of the properties of the living systems. To date, deriving an accurate correlation between the architectural characteristics of the bottlebrushes and their physical properties still remain a significant challenge despite an enormous progress in

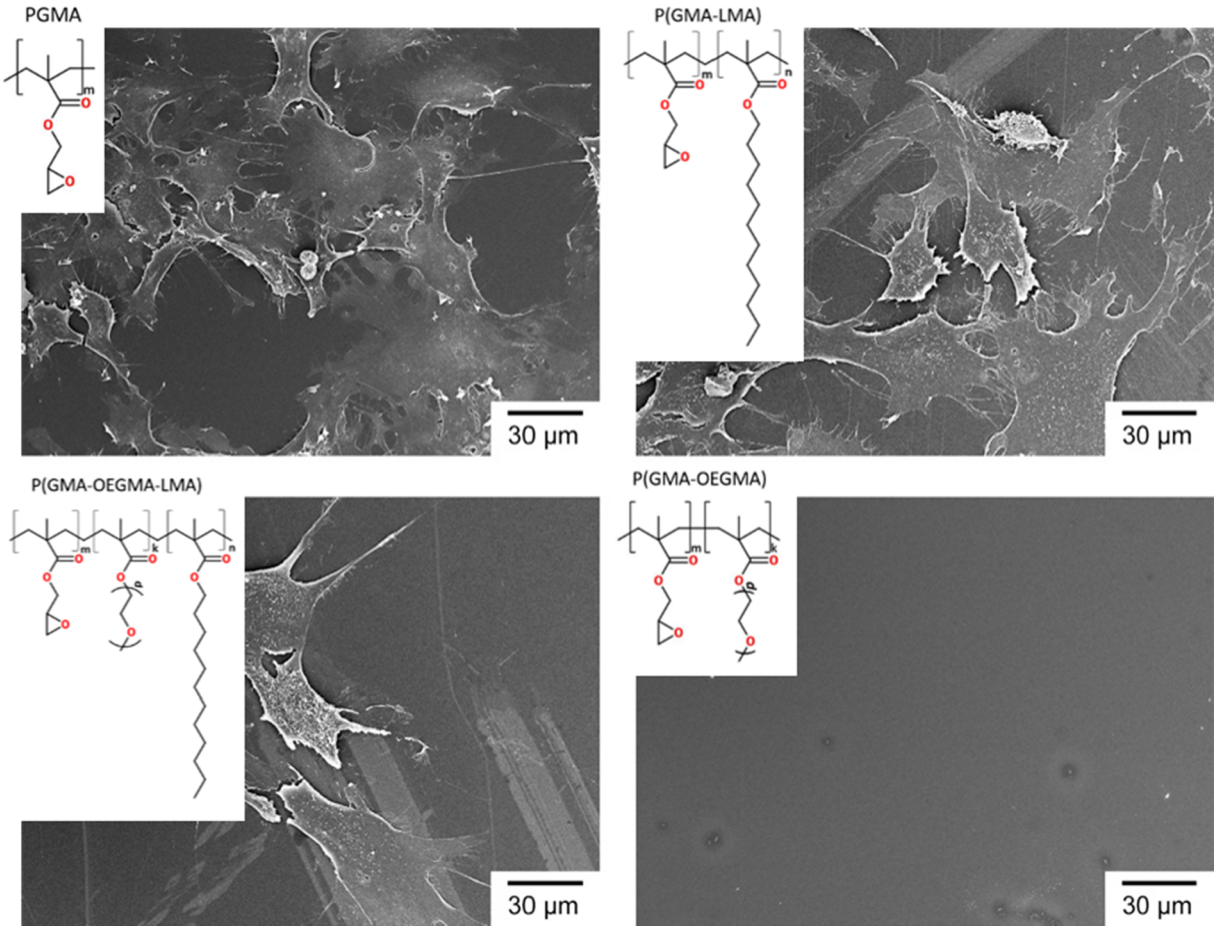

Fig. 10. The scanning electron micrographs of the osteoblasts attached to the silicon wafers coated with: PGMA and P(GMA_{26}-LMA_{74}) (top row) , and P(GMA_{15}-$OEGMA_{66}$-LMA_{19}) and P(GMA_{66}-$OEGMA_{34}$) (bottom row). Reprinted with permission from Ref. [62]. Copyright (2018) Americal Chemical Society.

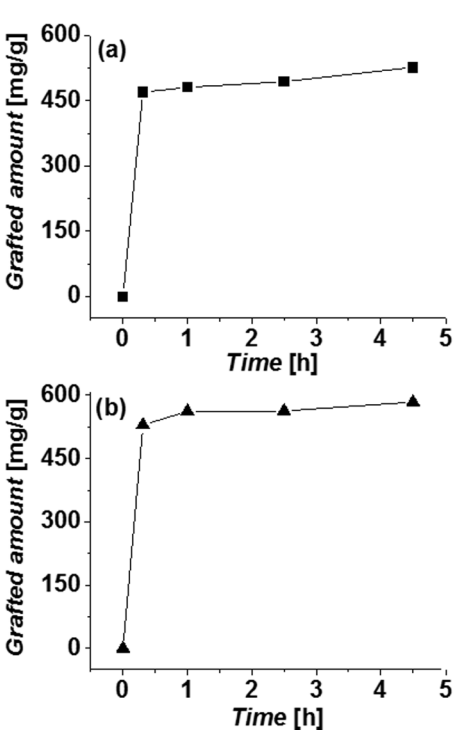

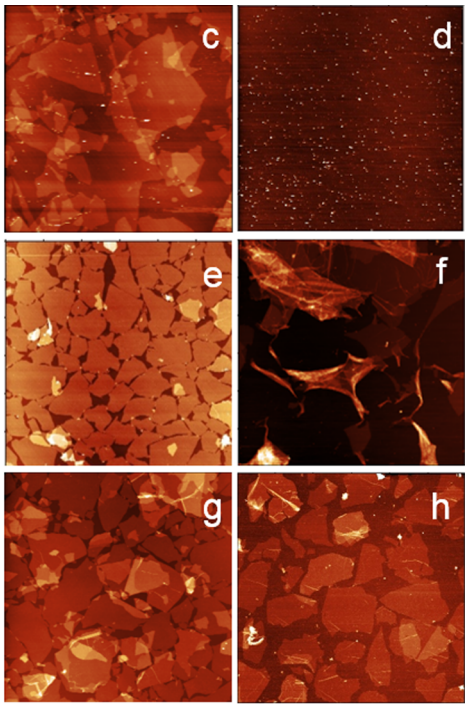

Fig. 11. Amount of molecular bottlebrushes (mg of MBB per gram of MBB/GO) grafted to GO from water as a function of time: (a) P(GMA_{66}-$OEGMA_{34}$) MBB and (b) P(GMA_{15}-$OEGMA_{66}$-LMA_{19}) MBB. Atomic force microscopy of pristine graphene oxide deposited on hydrophilic (c) and hydrophobic (d) surface, GO/P(GMA_{66}-$OEGMA_{34}$) on hydrophilic (e) and hydrophobic (f) surface and GO/P(GMA_{15}-$OEGMA_{66}$-LMA_{19}) on hydrophilic (g) and hydrophobic (h) surface. The size of the scans is 30 × 30 μm, vertical scale is 30 nm in (c), 2 nm in (d), 10 nm in (e, g, h), and 70 nm in (f). GO was deposited by the dip-coating from water. Reprinted (adapted) with permission from Ref. [62]. Copyright (2018) Americal Chemical Society.

ARTICLE IN PRESS

theoretical and computational studies of MBBs. This challenge stem from the numerous interactions on different length scales. Nevertheless, the markedly unique MBB chain architectures have led to a number of their exclusive applications owing to the bottlebrush distinctive chain size and flexibility, spatial conformations, interfacial activity, relatively fast self-assembly, multifunctionality, and low entanglement. We anticipate that the future developments in this area will be directed towards precise understanding and tailoring of the bottlebrush structure-properties relationships, utilization of MBBs as components of larger conjugated systems, and formalizing MBB materials as a distinct and mature industrial applications-ready field of polymer science and engineering.

Acknowledgements

O.K. gratefully acknowledges the National Science Foundation EPSCoR Program Award No. OIA-1655740 for partial funding of Sidong Tu.

References

[1] N. Zhang, S. Huber, A. Schulz, R. Luxenhofer, R. Jordan, Cylindrical molecular brushes of poly(2-oxazoline)s from 2-isopropenyl-2-oxazoline, Macromolecules 42 (6) (2009) 2215–2221.
[2] S. Panyukov, E.B. Zhulina, S.S. Sheiko, G.C. Randall, J. Brock, M. Rubinstein, Tension amplification in molecular brushes in solutions and on substrates, J. Phys. Chem. B 113 (12) (2009) 3750–3768.
[3] M. Wintermantel, M. Gerle, K. Fischer, M. Schmidt, I. Wataoka, H. Urakawa, K. Kajiwara, Y. Tsukahara, Molecular bottlebrushes, Macromolecules 29 (3) (1996) 978–983.
[4] J. Rzayev, Molecular bottlebrushes: new opportunities in nanomaterials fabrication, ACS Macro Lett. 1 (9) (2012) 1146–1149.
[5] A. Allen, Mucus—a protective secretion of complexity, Trends Biochem. Sci. 8 (5) (1983) 169–173.
[6] H.-P. Hsu, W. Paul, S. Rathgeber, K. Binder, Characteristic length scales and radial monomer density profiles of molecular bottle-brushes: simulation and experiment, Macromolecules 43 (3) (2010) 1592–1601.
[7] M. Mullner, A.H.E. Muller, Cylindrical polymer brushes – anisotropic building blocks, unimolecular templates and particulate nanocarriers, Polymer 98 (2016) 389–401.
[8] T. Pelras, C.S. Mahon, M. Mullner, Synthesis and applications of compartmentalised molecular polymer brushes, Angew. Chem.-Int. Ed. 57 (24) (2018) 6982–6994.
[9] D.P. Armstrong, R.J. Spontak, Designing dielectric elastomers over multiple length scales for 21st century soft materials technologies, Rubber Chem. Technol. 90 (2) (2017) 207–224.
[10] R. Verduzco, X.Y. Li, S.L. Pesek, G.E. Stein, Structure, function, self-assembly, and applications of bottlebrush copolymers (vol 44, pg 2405, 2015), Chem. Soc. Rev. 44 (21) (2015) 7916–7916.
[11] K. Matyjaszewski, Advanced materials by atom transfer radical polymerization, Adv. Mater. 30 (23) (2018).
[12] M. Vatankhah-Varnoosfaderani, W.F.M. Daniel, A.P. Zhushma, Q. Li, B.J. Morgan, K. Matyjaszewski, D.P. Armstrong, R.J. Spontak, A.V. Dobrynin, S.S. Sheiko, Bottlebrush elastomers: a new platform for freestanding electroactuation, Adv. Mater. 29 (2) (2017).
[13] J. Paturej, S.S. Sheiko, S. Panyukov, M. Rubinstein, Molecular structure of bottlebrush polymers in melts, Sci. Adv. 2 (11) (2016) 12.
[14] W.F.M. Daniel, J. Burdynska, M. Vatankhah-Varnoosfaderani, K. Matyjaszewski, J. Paturej, M. Rubinstein, A.V. Dobrynin, S.S. Sheiko, Solvent-free, supersoft and superelastic bottlebrush melts and networks, Nat. Mater. 15 (2) (2016) 183–189.
[15] O.V. Borisov, T.M. Birshtein, Y.B. Zhulina, The temperature-concentration diagram of state for solutions of comb-like macromolecules, Polymer Sci. U.S.S.R. 29 (7) (1987) 1552–1559.
[16] G.H. Fredrickson, Surfactant-induced lyotropic behavior of flexible polymer solutions, Macromolecules 26 (11) (1993) 2825–2831.
[17] L. Feuz, F.A.M. Leermakers, M. Textor, O. Borisov, Bending rigidity and induced persistence length of molecular bottle brushes: a self-consistent-field theory, Macromolecules 38 (21) (2005) 8891–8901.
[18] K. Binder, H.-P. Hsu, W. Paul, Understanding the stiffness of macromolecules: from linear chains to bottle-brushes, Eur. Phys. J. Special Topics 225 (8) (2016) 1663–1671.
[19] D. Chatterjee, T.A. Vilgis, Scaling laws of bottle-brush polymers in dilute solutions, Macromol. Theory Simulat. 25 (6) (2016) 518–523.
[20] H. Liang, S.S. Sheiko, A.V. Dobrynin, Supersoft and hyperelastic polymer networks with brushlike strands, Macromolecules 51 (2) (2018) 638–645.
[21] H. Liang, Z. Cao, Z. Wang, S.S. Sheiko, A.V. Dobrynin, Combs and bottlebrushes in a melt, Macromolecules 50 (8) (2017) 3430–3437.
[22] A. Chremos, J.F. Douglas, A comparative study of thermodynamic, conformational, and structural properties of bottlebrush with star and ring polymer melts, J. Chem. Phys. 149 (4) (2018) 044904.
[23] M.F. Zhang, A.H.E. Muller, Cylindrical polymer brushes, J. Polym. Sci. Part a-Polym. Chem. 43 (16) (2005) 3461–3481.
[24] S.S. Sheiko, B.S. Sumerlin, K. Matyjaszewski, Cylindrical molecular brushes: synthesis, characterization, and properties, Progr. Polym. Sci. 33 (7) (2008) 759–785.
[25] H.I. Lee, J. Pietrasik, S.S. Sheiko, K. Matyjaszewski, Stimuli-responsive molecular brushes, Progr. Polym. Sci. 35 (1–2) (2010) 24–44.
[26] M. Mullner, Molecular polymer brushes in nanomedicine, Macromol. Chem. Phys. 217 (20) (2016) 2209–2222.
[27] L.T. Strover, J. Malmstrom, J. Travas-Sejdic, Graft copolymers with conducting polymer backbones: a versatile route to functional materials, Chem. Rec. 16 (1) (2016) 393–418.
[28] Y.M. Chen, Shaped hairy polymer nanoobjects, Macromolecules 45 (6) (2012) 2619–2631.
[29] T.M. Birshtein, O.V. Borisov, Y.B. Zhulina, A.R. Khokhlov, T.A. Yurasova, Conformations of comb-like macromolecules, Vysokomolekulyarnye Soedineniya Seriya A 29 (6) (1987) 1169–1174.
[30] P.E. Theodorakis, H.-P. Hsu, W. Paul, K. Binder, Computer simulation of bottlebrush polymers with flexible backbone: good solvent versus theta solvent conditions, J. Chem. Phys. 135 (16) (2011).
[31] H. Hsiao-Ping, P. Wolfgang, B. Kurt, Understanding the multiple length scales describing the structure of bottle-brush polymers by Monte Carlo simulation methods, Macromol. Theory Simul. 20 (7) (2011) 510–525.
[32] J. Paturej, T. Kreer, Hierarchical excluded volume screening in solutions of bottlebrush polymers, Soft Matter 13 (45) (2017) 8534–8541.
[33] S. Elli, F. Ganazzoli, E.G. Timoshenko, Y.A. Kuznetsov, R. Connolly, Size and persistence length of molecular bottle-brushes by Monte Carlo simulations, J. Chem. Phys. 120 (13) (2004) 6257–6267.
[34] P.G. de Gennes, Scaling Concepts in Polymer Physics, Cornell University Press, 1979.
[35] M. Pannuzzo, R.D. Tilton, M. Deserno, Responsive behavior of a branched-chain polymer network: a molecular dynamics study, Soft Matter 14 (31) (2018) 6485–6495.
[36] H. Liang, B.J. Morgan, G. Xie, M.R. Martinez, E.B. Zhulina, K. Matyjaszewski, S.S. Sheiko, A.V. Dobrynin, Universality of the entanglement plateau modulus of comb and bottlebrush polymer melts, Macromolecules 51 (23) (2018) 10028–10039.
[37] M. Hu, Y. Xia, G.B. McKenna, J.A. Kornfield, R.H. Grubbs, Linear rheological response of a series of densely branched brush polymers, Macromolecules 44 (17) (2011) 6935–6943.
[38] S.J. Dalsin, M.A. Hillmyer, F.S. Bates, Linear rheology of polyolefin-based bottlebrush polymers, Macromolecules 48 (13) (2015) 4680–4691.
[39] I.N. Haugan, M.J. Maher, A.B. Chang, T.-P. Lin, R.H. Grubbs, M.A. Hillmyer, F.S. Bates, Consequences of grafting density on the linear viscoelastic behavior of graft polymers, ACS Macro Lett. 7 (5) (2018) 525–530.
[40] M. Jacobs, H. Liang, B. Pugnet, A.V. Dobrynin, Molecular dynamics simulations of surface and interfacial tension of graft polymer melts, Langmuir (2018).
[41] S.J. Dalsin, T.G. Rions-Maehren, M.D. Beam, F.S. Bates, M.A. Hillmyer, M.W. Matsen, Bottlebrush block polymers: quantitative theory and experiments, ACS Nano 9 (12) (2015) 12233–12245.
[42] M. Saariaho, O. Ikkala, I. Szleifer, I. Erukhimovich, G. tenBrinke, On lyotropic behavior of molecular bottle-brushes: a Monte Carlo computer simulation study, J. Chem. Phys. 107 (8) (1997) 3267–3276.
[43] L.T. Yan, Y.Y. Xu, M. Ballauff, A.H.E. Muller, A. Boker, Influence of counterion valency on the conformational behavior of cylindrical polyelectrolyte brushes, J. Phys. Chem. B 113 (15) (2009) 5104–5110.
[44] L.T. Yan, X.J. Zhang, Dissipative particle dynamics simulations of complexes comprised of cylindrical polyelectrolyte brushes and oppositely charged linear polyelectrolytes, Langmuir 25 (6) (2009) 3808–3813.
[45] C.-Y. Teng, Y.-J. Sheng, H.-K. Tsao, Boundary-induced segregation in nanoscale thin films of athermal polymer blends, Soft Matter 12 (20) (2016) 4603–4610.
[46] H.-P. Hsu, W. Paul, K. Binder, Scattering function of semiflexible polymer chains under good solvent conditions, J. Chem. Phys. 137 (17) (2012) 174902.
[47] T. Norisuye, H. Fujita, Excluded-volume effects in dilute polymer solutions. XIII. Effects of chain stiffness, Polym. J. 14 (2) (1982) 143.
[48] G.M. Leuty, M. Tsige, G.S. Grest, M. Rubinstein, Tension amplification in tethered layers of bottle-brush polymers, Macromolecules 49 (5) (2016) 1950–1960.
[49] S.S. Sheiko, S. Panyukov, M. Rubinstein, Bond tension in tethered macromolecules, Macromolecules 44 (11) (2011) 4520–4529.
[50] Z. Zhang, J.-M.Y. Carrillo, S.-K. Ahn, B. Wu, K. Hong, G.S. Smith, C. Do, Atomistic structure of bottlebrush polymers: simulations and neutron scattering studies, Macromolecules 47 (16) (2014) 5808–5814.
[51] A. Chremos, P.E. Theodorakis, Morphologies of bottle-brush block copolymers, ACS Macro Lett. 3 (10) (2014) 1096–1100.
[52] W. Gu, J. Huh, S.W. Hong, B.R. Sveinbjornsson, C. Park, R.H. Grubbs, T.P. Russell, Self-assembly of symmetric brush diblock copolymers, ACS Nano 7 (3) (2013) 2551–2558.
[53] R.D. Groot, P.B. Warren, Dissipative particle dynamics: bridging the gap between atomistic and mesoscopic simulation, J. Chem. Phys. 107 (11) (1997) 4423–4435.
[54] P. Español, P.B. Warren, Perspective: dissipative particle dynamics, J. Chem. Phys. 146 (15) (2017) 150901.
[55] C.K. Choudhury, O. Kuksenok, Modeling dynamics of polyacrylamide gel in oil-water mixtures: dissipative particle dynamics approach, MRS Adv. 3 (26) (2018) 1469–1474.
[56] A.L. Liberman-Martin, C.K. Chu, R.H. Grubbs, Application of bottlebrush block copolymers as photonic crystals, Macromol. Rapid Commun. 38 (13) (2017).

ARTICLE IN PRESS

[57] H. Unsal, S. Onbulak, F. Calik, M. Er-Rafik, M. Schmutz, A. Sanyal, J. Rzayev, Interplay between molecular packing, drug loading, and core cross-linking in bottlebrush copolymer micelles, Macromolecules 50 (4) (2017) 1342–1352.

[58] X.Y. Tu, C. Meng, X.L. Zhang, M.G. Jin, X.S. Zhang, X.Z. Zhao, Y.F. Wang, L.W. Ma, B.Y. Wang, M.Z. Liu, H. Wei, Fabrication of reduction-sensitive amphiphilic cyclic brush copolymer for controlled drug release, Macromol. Biosci. 18 (7) (2018).

[59] D. Ndaya, R. Bosire, L. Mahajan, S. Huh, R. Kasi, Synthesis of ordered, functional, robust nanoporous membranes from liquid crystalline brush-like triblock copolymers, Polym. Chem. 9 (12) (2018) 1404–1411.

[60] P. Deshmukh, H. Yoon, S. Cho, S.Y. Yoon, O.V. Zore, T. Kim, I. Chung, S.K. Ahn, R.M. Kasi, Impact of poly(-caprolactone) architecture on the thermomechanical and shape memory properties, J. Polym. Sci. Part A-Polym. Chem. 55 (20) (2017) 3424–3433.

[61] Y.W. Xu, W.Y. Wang, Y.Y. Wang, J.H. Zhu, D. Uhrig, X.Y. Lu, J.K. Keum, J.W. Mays, K.L. Hong, Fluorinated bottlebrush polymers based on poly(trifluoroethyl methacrylate): synthesis and characterization, Polym. Chem. 7 (3) (2016) 680–688.

[62] N. Borodinov, D. Gil, M. Savchak, C.E. Gross, N.S. Yadavalli, R.L. Ma, V.V. Tsukruk, S. Minko, A. Vertegel, I. Luzinov, En route to practicality of the polymer grafting technology: one-step interfacial modification with amphiphilic molecular brushes, ACS Appl. Mater. Interfaces 10 (16) (2018) 13941–13952.

[63] M. Savchak, N. Borodinov, R. Burtovyy, M. Anayee, K.S. Hu, R.L. Ma, A. Grant, H.M. Li, D.B. Cutshall, Y.M. Wen, G. Koley, W.R. Harrell, G. Chumanov, V. Tsukruk, I. Luzinov, Highly conductive and transparent reduced graphene oxide nanoscale films via thermal conversion of polymer-encapsulated graphene oxide sheets, ACS Appl. Mater. Interfaces 10 (4) (2018) 3975–3985.

[64] S.L. Pesek, Y.H. Lin, H.Z. Mah, W. Kasper, B. Chen, B.J. Rohde, M.L. Robertson, G.E. Stein, R. Verduzco, Synthesis of bottlebrush copolymers based on poly(dimethylsiloxane) for surface active additives, Polymer 98 (2016) 495–504.

[65] M. Vatankhah-Varnosfaderani, A.N. Keith, Y. Cong, H. Liang, M. Rosenthal, M. Sztucki, C. Clair, S. Magonov, D.A. Ivanov, A.V. Dobrynin, S.S. Sheiko, Chameleon-like elastomers with molecularly encoded strain-adaptive stiffening and coloration, Science 359 (6383) (2018) 1509.

[66] J. Motoyanagi, T. Ishikawa, M. Minoda, Stimuli-responsive brush-shaped conjugated polymers with pendant well-defined poly(vinyl ether)s, J. Polym. Sci. Part A-Polym. Chem. 54 (20) (2016) 3318–3325.

[67] B.B. Xu, X.W. Sun, C.Q. Wu, J.H. Hu, X.Y. Huang, Construction of catechol-containing semi-fluorinated asymmetric polymer brush via successive RAFT polymerization and ATRP, Polym. Chem. 8 (48) (2017) 7499–7506.

[68] A. Cappelli, M. Paolino, G. Grisci, V. Razzano, G. Giuliani, A. Donati, C. Bonechi, R. Mendichi, S. Battiato, F. Samperi, C. Scialabba, G. Giammona, F. Makovec, M. Licciardi, Hyaluronan-coated polybenzofulvene brushes as biomimetic materials, Polym. Chem. 7 (42) (2016) 6529–6544.

[69] J.M. Ren, J. Subbiah, B. Zhang, K. Ishitake, K. Satoh, M. Kamigaito, G.G. Qiao, E.H.H. Wong, W.W.H. Wong, Fullerene peapod nanoparticles as an organic semiconductor-electrode interface layer, Chem. Commun. 52 (16) (2016) 3356–3359.

[70] D. van As, J. Subbiah, D.J. Jones, W.W.H. Wong, Controlled synthesis of well-defined semiconducting brush polymers, Macromol. Chem. Phys. 217 (3) (2016) 403–413.

[71] N.S. Yadavalli, N. Borodinov, C. Choudhury, T. Quiñones-Ruiz, A. Laradji, S. Tu, I. Lednev, O. Kuksenok, I. Luzinov, S. Minko, Thermal stabilization of enzymes with molecular brushes, ACS Catal. 7 (12) (2017) 8675–8684.

[72] J.M. Sarapas, E.P. Chan, E.M. Rettner, K.L. Beers, Compressing and swelling to study the structure of extremely soft bottlebrush networks prepared by ROMP, Macromolecules 51 (6) (2018) 2359–2366.

[73] G.J. Xie, P. Krys, R.D. Tilton, K. Matyjaszewski, Heterografted molecular brushes as stabilizers for water-in-oil emulsions, Macromolecules 50 (7) (2017) 2942–2950.

[74] X.Y. Tu, C. Meng, Y.F. Wang, L.W. Ma, B.Y. Wang, J.L. He, P.H. Ni, X.L. Ji, M.Z. Liu, H. Wei, Fabrication of thermosensitive cyclic brush copolymer with enhanced therapeutic efficacy for anticancer drug delivery, Macromol. Rapid Commun. 39 (5) (2018).

[75] J. Faivre, B.R. Shrestha, G.J. Xie, M. Olszewski, V. Adibnia, F. Moldovan, A. Montembault, G. Sudre, T. Delair, L. David, K. Matyjaszewski, X. Banquy, Intermolecular interactions between bottlebrush polymers boost the protection of surfaces against frictional wear, Chem. Mater. 30 (12) (2018) 4140–4149.

[76] L.L.C. Olijve, M. Hendrix, I.K. Voets, Influence of polymer chain architecture of poly (vinyl alcohol) on the inhibition of ice recrystallization, Macromol. Chem. Phys. 217 (8) (2016) 951–958.

[77] B.B. Xu, C. Feng, J.H. Hu, P. Shi, G.X. Gu, L. Wang, X.Y. Huang, Spin-casting polymer brush films for stimuli-responsive and anti-fouling surfaces, ACS Appl. Mater. Interfaces 8 (10) (2016) 6685–6692.

[78] S. Wang, C.G. Liu, H. Zhou, C.Q. Gao, W.Q. Zhang, An efficient route to synthesize thermoresponsive molecular bottlebrushes of poly o-aminobenzyl alcohol-graft-poly(N-isopropylacrylamide), Polym. Chem. 8 (12) (2017) 1932–1942.

[79] M. Mullner, K. Yang, A. Kaur, E.J. New, Aspect-ratio-dependent interaction of molecular polymer brushes and multicellular tumour spheroids, Polym. Chem. 9 (25) (2018) 3461–3465.

[80] Y.F. Lyu, Z.J. Zhang, C. Liu, Z. Geng, L.C. Gao, Q. Chen, Random binary brush architecture enhances both ionic conductivity and mechanical strength at room temperature, Chinese J. Polym. Sci. 36 (1) (2018) 78–84.

[81] B.B. Jiang, Y.J. He, B. Li, S.Q. Zhao, S. Wang, Y.B. He, Z.Q. Lin, Polymer-templated formation of polydopamine-coated SnO2 nanocrystals: anodes for cyclable lithium-ion batteries, Angew. Chem.-Int. Ed. 56 (7) (2017) 1869–1872.

[82] M. Abbasi, L. Faust, K. Riazi, M. Wilhelm, Linear and extensional rheology of model branched polystyrenes: from loosely grafted combs to bottlebrushes, Macromolecules 50 (15) (2017) 5964–5977.

[83] R. Yuan, M. Kopec, G.J. Xie, E. Gottlieb, J.W. Mohin, Z.Y. Wang, M. Lamson, T. Kowalewski, K. Matyjaszewski, Mesoporous nitrogen-doped carbons from PAN-based molecular bottlebrushes, Polymer 126 (2017) 352–359.

[84] M.H. Zhou, H. Zhang, L.F. Xiong, Z.D. He, T.Q. Wang, Y. Xu, K. Huang, Fe-Porphyrin functionalized microporous organic nanotube networks and their application for the catalytic olefination of aldehydes and carbene insertion into N-H bonds, Polym. Chem. 8 (24) (2017) 3721–3730.

[85] M.H. Zhou, H. Zhang, L.F. Xiong, Z.D. He, A.Q. Zhong, T.Q. Wang, Y. Xu, K. Huang, Synthesis of magnetic microporous organic nanotube networks for adsorption application, RSC Adv. 6 (90) (2016) 87745–87752.

[86] J. Rzayev, Synthesis of polystyrene − polylactide bottlebrush block copolymers and their melt self-assembly into large domain nanostructures, Macromolecules 42 (6) (2009) 2135–2141.

[87] C.D. Heinrich, M. Thelakkat, Poly-(3-hexylthiophene) bottlebrush copolymers with tailored side-chain lengths and high charge carrier mobilities, J. Mater. Chem. C 4 (23) (2016) 5370–5378.

[88] I. Gadwal, J.Y. Rao, J. Baettig, A. Khan, Functionalized molecular bottlebrushes, Macromolecules 47 (1) (2014) 35–40.

[89] A.C. Engler, H.I. Lee, P.T. Hammond, Highly efficient “grafting onto” a polypeptide backbone using click chemistry, Angew. Chem.-Int. Ed. 48 (49) (2009) 9334–9338.

[90] D. Lanson, F. Ariura, M. Schappacher, R. Borsali, A. Deffieux, Comb copolymers with polystyrene and polyisoprene branches: effect of block topology on film morphology, Macromolecules 42 (12) (2009) 3942–3950.

[91] G. Zardalidis, A. Pipertzis, G. Mountrichas, S. Pispas, M. Mezger, G. Floudas, Effect of polymer architecture on the ionic conductivity. densely grafted poly(ethylene oxide) brushes doped with LiTf, Macromolecules 49 (7) (2016) 2679–2687.

[92] M. Ina, Z. Cao, M. Vatankhah-Varnoosfaderani, M.H. Everhart, W.F.M. Daniel, A.V. Dobrynin, S.S. Sheiko, From adhesion to wetting: contact mechanics at the surfaces of super-soft brush-like elastomers, ACS Macro Lett. 6 (8) (2017) 854–858.

[93] C. Vieille, G.J. Zeikus, Hyperthermophilic enzymes: sources, uses, and molecular mechanisms for thermostability, Microbiol. Mol. Biol. Rev. 65 (1) (2001) 1–43.

[94] P.V. Iyer, L. Ananthanarayan, Enzyme stability and stabilization—aqueous and non-aqueous environment, Process Biochem. 43 (10) (2008) 1019–1032.

[95] C.K. Choudhury, S. Tu, I. Luzinov, S. Minko, O. Kuksenok, Designing highly thermostable lysozyme-copolymer conjugates: focus on effect of polymer concentration, Biomacromolecules 19 (4) (2018) 1175–1188.

[96] X. Wang, N.S. Yadavalli, A.M. Laradji, S. Minko, Grafting through method for implanting of lysozyme enzyme in molecular brush for improved biocatalytic activity and thermal stability, Macromolecules 51 (14) (2018) 5039–5047.

[97] J.M. Ren, K. Ishitake, K. Satoh, A. Blencowe, Q. Fu, E.H.H. Wong, M. Kamigaito, G.G. Qiao, Stereoregular high-density bottlebrush polymer and its organic nanocrystal stereocomplex through triple-helix formation, Macromolecules 49 (3) (2016) 788–795.

[98] C.G. Chae, Y.G. Yu, M.J. Kim, R.H. Grubbs, J.S. Lee, Experimental formulation of photonic crystal properties for hierarchically self-assembled POSS-bottlebrush block copolymers, Macromolecules 51 (9) (2018) 3458–3466.

[99] Y.J. Su, Z.L. Zhi, Q. Gao, M.H. Xie, M. Yu, B. Lei, P. Li, P.X. Ma, Autoclaving-derived surface coating with in vitro and in vivo antimicrobial and antibiofilm efficacies, Adv. Healthcare Mater. 6 (6) (2017).